Measurement of the branching fractions of the decays $D^+ \to K^-K^+K^+$, $D^+ \to \pi^-\pi^+K^+$ and $D^+\_s \to \pi^-K^+K^+$

Roel Aaij, Carlos Abellán Beteta, Bernardo Adeva, Marco Adinolfi, Christine Angela Aidala, Ziad Ajaltouni, Simon Akar, Pietro Albicocco, Johannes Albrecht, Federico Alessio, et al.

Published for SISSA by Springer

Received: October 11, 2018
Revised: February 8, 2019
Accepted: March 5, 2019
Published: March 27, 2019

Measurement of the branching fractions of the decays $D^+ \to K^-K^+K^+$, $D^+ \to \pi^-\pi^+K^+$ and $D_s^+ \to \pi^-K^+K^+$

The LHCb collaboration

E-mail: poly@if.ufrj.br

Abstract: The branching fractions of the doubly Cabibbo-suppressed decays $D^+ \to K^-K^+K^+$, $D^+ \to \pi^-\pi^+K^+$ and $D_s^+ \to \pi^-K^+K^+$ are measured using the decays $D^+ \to K^-\pi^+\pi^+$ and $D_s^+ \to K^-K^+\pi^+$ as normalisation channels. The measurements are performed using proton-proton collision data collected with the LHCb detector at a centre-of-mass energy of 8 TeV, corresponding to an integrated luminosity of $2.0\,\text{fb}^{-1}$. The results are

$$\frac{\mathcal{B}(D^+ \to K^-K^+K^+)}{\mathcal{B}(D^+ \to K^-\pi^+\pi^+)} = (6.541 \pm 0.025 \pm 0.042) \times 10^{-4},$$
$$\frac{\mathcal{B}(D^+ \to \pi^-\pi^+K^+)}{\mathcal{B}(D^+ \to K^-\pi^+\pi^+)} = (5.231 \pm 0.009 \pm 0.023) \times 10^{-3},$$
$$\frac{\mathcal{B}(D_s^+ \to \pi^-K^+K^+)}{\mathcal{B}(D_s^+ \to K^-K^+\pi^+)} = (2.372 \pm 0.024 \pm 0.025) \times 10^{-3},$$

where the uncertainties are statistical and systematic, respectively. These are the most precise measurements up to date.

Keywords: Branching fraction, Charm physics, Flavor physics, Hadron-Hadron scattering (experiments)

ArXiv ePrint: 1810.03138

https://doi.org/10.1007/JHEP03(2019)176

JHEP03(2019)176

Contents

JHEP03(2019)176

1 Introduction

Precise measurements of the branching fractions of doubly Cabibbo-suppressed (DCS) decays of charmed mesons provide important information for the understanding of the decay dynamics of these particles. The theoretical description of charm-meson decays is challenging. The charm quark is not heavy enough for a reliable application of the factorisation approach and heavy-quark expansion tools, successfully used in B-meson decays. It is also not light enough for the application of chiral perturbation theory, as in the case of kaon decays. Phenomenological models and approximate symmetries, such as those based on the diagrammatic approach [1, 2], rely on the knowledge of branching fractions and, in the case of multi-body final states, resonant structures, as key inputs. Whilst the branching fractions of some decay modes of charmed mesons are well measured, the uncertainties on branching fractions of doubly Cabibbo-suppressed decays are still large.

In this paper, three ratios of branching fractions of DCS decays of D^+ and D_s^+ mesons[1] are measured with unprecedented precision,

$$\frac{\mathcal{B}(D^+ \to K^-K^+K^+)}{\mathcal{B}(D^+ \to K^-\pi^+\pi^+)}, \quad \frac{\mathcal{B}(D^+ \to \pi^-\pi^+K^+)}{\mathcal{B}(D^+ \to K^-\pi^+\pi^+)}, \quad \frac{\mathcal{B}(D_s^+ \to \pi^-K^+K^+)}{\mathcal{B}(D_s^+ \to K^-K^+\pi^+)}. \tag{1.1}$$

In addition, the branching fraction of the Cabibbo-suppressed (CS) $D^+ \to K^-K^+\pi^+$ decay is measured relative to that of the Cabibbo-favoured (CF) $D^+ \to K^-\pi^+\pi^+$ decay.

[1] Throughout this paper, charge conjugated decays are implied.

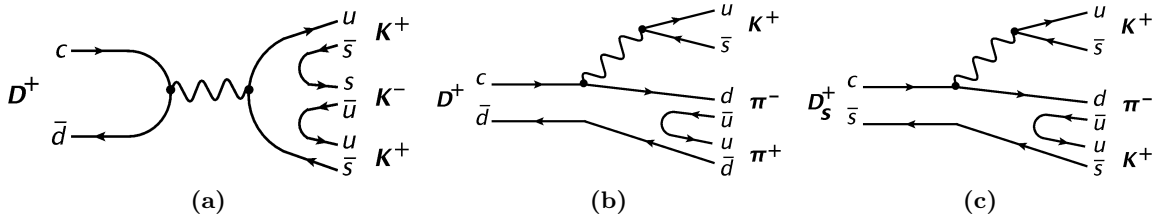

Figure 1. Feynman diagrams for the DCS decays (a) $D^+ \to K^-K^+K^+$, (b) $D^+ \to \pi^-\pi^+K^+$ and (c) $D_s^+ \to \pi^-K^+K^+$.

Ratio	Value $[\times 10^{-3}]$
$\mathcal{B}(D^+ \to K^-K^+K^+)/\mathcal{B}(D^+ \to K^-\pi^+\pi^+)$	0.95 ± 0.22
$\mathcal{B}(D^+ \to \pi^-\pi^+K^+)/\mathcal{B}(D^+ \to K^-\pi^+\pi^+)$	5.77 ± 0.22
$\mathcal{B}(D_s^+ \to \pi^-K^+K^+)/\mathcal{B}(D_s^+ \to K^-K^+\pi^+)$	2.33 ± 0.23
$\mathcal{B}(D^+ \to K^-K^+\pi^+)/\mathcal{B}(D^+ \to K^-\pi^+\pi^+)$	105.9 ± 1.8

Table 1. World averages for the branching-fractions ratios under consideration [3].

Tree-level diagrams for the three DCS decays are exemplified in figure 1, where the final state particles can be produced through resonances not explicitly shown. The decay $D^+ \to K^-K^+K^+$ is expected to occur through an annihilation process as in figure 1a but it is also possible to produce the $K^-K^+K^+$ final state through a diagram similar to that in figure 1b, where a K^+K^- pair could be formed through the $K^0\overline{K}^0 \to K^+K^-$ rescattering or through a resonance that couples to both $d\bar{d}$ and $s\bar{s}$.

The world averages [3] of these ratios of branching fractions are listed in table 1. In the case of the $D^+ \to K^-K^+K^+$ decay, there is only one previous measurement by the FOCUS collaboration [4], based on a sample of 65 ± 15 decays and with a precision of 23%.

The results presented in this paper are obtained with a sample of pp-collision data corresponding to an integrated luminosity of $2.0\,\text{fb}^{-1}$, collected at a centre-of-mass energy of 8 TeV with the LHCb detector. In section 2 a description of the detector and simulation is presented. The method used to measure the ratio of branching fractions is described in section 3. The selection is discussed in section 4. The determination of the efficiencies in bins of the phase space is explained in section 5. The fit model and the evaluation of the signal yields are presented in section 6. Systematic uncertainties associated with the measurements are discussed in section 7. Finally, the results and conclusions are presented in section 8.

2 Detector and simulation

The LHCb detector [5, 6] is a single-arm forward spectrometer covering the pseudorapidity range $2 < \eta < 5$, designed for the study of particles containing b or c quarks. The detector includes a high-precision tracking system consisting of a silicon-strip vertex detector surrounding the pp interaction region, a large-area silicon-strip detector located upstream of

JHEP03(2019)176

a dipole magnet with a bending power of about 4 Tm, and three stations of silicon-strip detectors and straw drift tubes placed downstream of the magnet. The tracking system provides a measurement of the momentum, p, of charged particles with a relative uncertainty that varies from 0.5% at low momentum to 1.0% at 200 GeV/c. The minimum distance of a track to a primary vertex (PV), the impact parameter (IP), is measured with a resolution of $(15 + 29/p_{\mathrm{T}})\,\mu$m, where p_{T} is the component of the momentum transverse to the beam, in GeV/c. Different types of charged hadrons are distinguished using information from two ring-imaging Cherenkov detectors [7]. Photons, electrons and hadrons are identified by a calorimeter system consisting of scintillating-pad and preshower detectors, an electromagnetic calorimeter and a hadronic calorimeter. Muons are identified by a system composed of alternating layers of iron and multiwire proportional chambers.

The polarity of the dipole magnet is reversed periodically throughout data taking. The configurations with the magnetic field upwards, *MagUp*, and downwards, *MagDown*, bend respectively positively and negatively charged particles in the horizontal plane towards the centre of the LHC.

The online event selection is performed by a trigger system [8], which consists of a hardware stage, based on information from the calorimeter and muon systems, followed by a software stage, which applies a full event reconstruction. At the hardware-trigger stage, events are required to have a muon with high p_{T} or a hadron, photon or electron with high transverse energy in the calorimeters. In the offline selection, the hardware trigger signals are associated with reconstructed particles. Selection requirements can therefore be made on whether the decision is due to the signal candidate, other particles produced in the pp collision, or a combination of both. The latter is used in this analysis. The software trigger is divided into two parts. The first part employs a partial reconstruction of the tracks, and a requirement on p_{T} and IP is applied to, at least, one final-state track forming the $D^+_{(s)}$ candidate. In the second part a full event reconstruction is performed and dedicated algorithms are used to select $D^+_{(s)}$ candidates decaying into three charged hadrons.

In the simulation, pp collisions are generated using Pythia [9] with a specific LHCb configuration [10]. Decays of hadronic particles are described by EvtGen [11], in which final-state radiation is generated using Photos [12]. The interaction of the generated particles with the detector, and its response, are implemented using the Geant4 toolkit [13] as described in ref. [14].

3 Method

The ratios of branching fractions are measured as

$$\frac{\mathcal{B}(D^+_{(s)} \to f_{\mathrm{signal}})}{\mathcal{B}(D^+_{(s)} \to f_{\mathrm{norm}})} = \frac{N^{\mathrm{prod}}_{\mathrm{signal}}}{N^{\mathrm{prod}}_{\mathrm{norm}}}, \tag{3.1}$$

where f_{signal} and f_{norm} correspond to the final states of the signal and normalisation $D^+_{(s)}$ decays, and $N^{\mathrm{prod}}_{\mathrm{signal}}$ and $N^{\mathrm{prod}}_{\mathrm{norm}}$ are the total number of produced signal and normalisation decays. These numbers are determined by correcting the observed yields of signal ($N^{\mathrm{obs}}_{\mathrm{signal}}$)

JHEP03(2019)176

and normalisation ($N^{\rm obs}_{\rm norm}$) decays after full selection criteria by the total respective efficiencies, which are obtained from simulation and from calibration data samples. Since there are no reliable decay amplitude models available for all the $D^+_{(s)} \to h^-_1 h^+_2 h^+_3$ decays,[2] the simulated samples are generated according to phase space distribution. As the efficiency, ε, is not uniform across the phase space, both the efficiency and the number of observed decays are obtained in bins of the Dalitz plot (DP) [15], built with two independent invariant masses squared, denoted as $s(h^-_1 h^+_2)$ and $s(h^-_1 h^+_3)$. The total number of produced decays is then evaluated as

$$N^{\rm prod} = \sum_i^{N_{\rm bins}} \frac{N^{\rm obs}_i}{\varepsilon_i}, \tag{3.2}$$

where the index i runs over the bins within the kinematically allowed region of the decay DP. When the decay has two identical particles in the final state, the DP is folded, with axes corresponding to the highest and lowest values of the two invariants, $s_{\rm hi}(h^- h'^+)$ and $s_{\rm lo}(h^- h'^+)$.

The distributions of both the efficiencies and observed yields over the phase space are obtained separately for statistically independent datasets split by magnet polarity. For each pair of signal and normalisation decays, the final experimental result is the combination of the *MagDown* and *MagUp* measurements of the ratio of branching fractions.

Systematic uncertainties are estimated using the ratios of observed yields $N^{\rm obs}_{\rm signal}/N^{\rm obs}_{\rm norm}$ and the ratios of average efficiencies, where the average is over the DP bins with weights given by the corresponding yields of observed candidates. They are also obtained separately for the different magnet polarities. The contributions from the relative uncertainties on the ratios of yields and on effective efficiencies are then added in quadrature to provide the relative uncertainty on each ratio of branching fractions.

4 Offline selection

The offline candidate selection reduces the combinatorial background and suppresses specific peaking structures in the various mass spectra. These structures are due to crossfeeds from decays of other charm particles, which occur when one or more final-state particles are misidentified or not reconstructed.

A first set of requirements exploits the decay topology by selecting combinations of three charged hadrons forming a good quality decay vertex, well detached from the PV. The PV is that with the smallest value of $\chi^2_{\rm IP}$, where $\chi^2_{\rm IP}$ is defined as the difference in the vertex-fit χ^2 of the PV reconstructed with and without the particle under consideration, in this case the $D^+_{(s)}$ candidate. The requirements at this level are made on the following quantities: the distance between the PV and the $D^+_{(s)}$ decay vertex; the IP of the $D^+_{(s)}$ candidate; the angle between the reconstructed $D^+_{(s)}$ momentum and the flight direction; the χ^2 of the $D^+_{(s)}$ decay vertex fit; the distance of closest approach between any two final-state tracks; and the momentum, the transverse momentum and the $\chi^2_{\rm IP}$ of the $D^+_{(s)}$

[2] Here h denotes a pion or a kaon and the particle ordering is such that h_1 has opposite charge with respect to the $D^+_{(s)}$ candidate.

JHEP03(2019)176

candidate and of its decay products. For each branching-fraction ratio measurement, signal and normalisation-channel candidates are selected with the same topology requirements, allowing a partial cancellation of the systematic uncertainties. Besides being effective to reduce combinatorial background, these topology criteria suppress the background from the decays $D^{*+} \to D^0\pi^+$, where the D^0 decays to two charged hadrons, such as $D^0 \to K^-\pi^+$ or $D^0 \to K^-\pi^+\pi^0$.

Particle identification (PID) criteria are used to distinguish between kaons and pions and to veto muons from semileptonic decays with two charged hadrons and a muon in the final state, such as the $D^+ \to K^-\pi^+\mu^+\nu_\mu$ decay. Further selection criteria based on more stringent PID requirements or invariant-mass vetoes are used to suppress crossfeeds contributing to each decay mode, except for the $D_s^+ \to \pi^-K^+K^+$ channel, which does not present this kind of contamination.

The two main crossfeeds in the $D^+ \to K^-K^+K^+$ channel are those from Λ_c^+ decays into K^-K^+p and $K^-p\pi^+$ final states. The former is the dominant contribution, in spite of being Cabibbo suppressed, since this background is caused by a single $p-K$ misidentification. These backgrounds are removed using invariant-mass vetoes. Candidates are reconstructed under the K^-K^+p and $K^-p\pi^+$ mass hypotheses and rejected if the resulting invariant masses are within $[2280, 2296]\,\mathrm{MeV}/c^2$. This veto is slightly different for other decay modes as the reconstructed width of the Λ_c^+ mass peak is affected by the decay channel-dependent selection criteria.

The main exclusive backgrounds for the $D^+ \to \pi^-\pi^+K^+$ decay are the fully reconstructed decays $D_s^+ \to K^-K^+\pi^+$, $D^+ \to K^-\pi^+\pi^+$, $\Lambda_c^+ \to \pi^-\pi^+p$ and $D^+ \to K_S^0K^+$, where K_S^0 decays to $\pi^-\pi^+$. The $D_s^+ \to K^-K^+\pi^+$ decay is the most abundant contamination, occurring when the K^+ meson is misidentified as a pion. The contamination from the decay $D^+ \to K^-\pi^+\pi^+$ is due to a double $K-\pi$ misidentification. These two backgrounds are suppressed by stringent PID requirements on the kaon and opposite-charge pion candidates. The crossfeed from the $\Lambda_c^+ \to \pi^-\pi^+p$ decays, on the other hand, is eliminated by an invariant-mass veto. The $p-K$ misidentification occurs mostly at high momenta, where the discrimination between these two particles is limited. Candidates are reconstructed under the $\pi^-\pi^+p$ hypothesis and rejected if their invariant mass is within the interval $[2275, 2300]\,\mathrm{MeV}/c^2$. The decay $D^+ \to K_S^0(\pi^-\pi^+)K^+$ has the same final state as the $D^+ \to \pi^-\pi^+K^+$ decay, hence this contamination cannot be suppressed using PID. In this case, candidates with $\pi^-\pi^+$ invariant mass within the interval $[488, 508]\,\mathrm{MeV}/c^2$ are discarded.

The main backgrounds in the $D_s^+ \to K^-K^+\pi^+$ sample are the $D^+ \to K^-\pi^+\pi^+$ and the $\Lambda_c^+ \to K^-p\pi^+$ decays. A stringent PID requirement on the K^+ candidate is used to suppress the contamination from $D^+ \to K^-\pi^+\pi^+$ decays, whereas an invariant-mass veto eliminates the $\Lambda_c^+ \to K^-p\pi^+$ background. The $K^-K^+\pi^+$ candidate is reconstructed as $K^-p\pi^+$ and the candidate is discarded if the resulting invariant mass is within $[2275, 2305]\,\mathrm{MeV}/c^2$.

The $\Lambda_c^+ \to K^-p\pi^+$ decay is the main specific background contribution in the $D^+ \to K^-K^+\pi^+$ sample. The $K^-K^+\pi^+$ candidates are reconstructed as $K^-p\pi^+$ and those with invariant mass within $[2275, 2305]\,\mathrm{MeV}/c^2$ are vetoed.

There are two backgrounds in the $D^+ \to K^-\pi^+\pi^+$ sample, the decays $D_s^+ \to K^-K^+\pi^+$ and $\Lambda_c^+ \to K^-p\pi^+$. To reject the Λ_c^+ background the $K^-\pi^+\pi^+$ candidates are recon-

JHEP03(2019)176

structed as $K^-p\pi^+$ and those with invariant mass within $[2280, 2300]\,\mathrm{MeV}/c^2$ are vetoed. The crossfeed from $D_s^+ \to K^-K^+\pi^+$ is suppressed using a stringent PID requirement on the pion candidate with the highest momentum.

5 Efficiencies

In order to take into account the variation of the efficiencies across the phase space, the measurement of the ratios of branching fractions in this analysis is based upon the correction of the observed yields in bins of the corresponding DP.

In each bin i of the DP, the overall selection efficiencies for signal and normalisation modes, ε_i in eq. (3.2), are factorised into components that are independently measured. The acceptance due to the detector geometry and the efficiencies due to trigger, final state particles reconstruction, offline selection and invariant-mass vetoes are obtained from simulation.

The PID efficiency of each candidate is estimated by multiplying the efficiencies for each final-state particle, which are evaluated from calibration samples of $D^0 \to K^-\pi^+$ decays [16] and depend on the particle momentum, pseudorapidity and event charged-particle multiplicity. Average PID efficiencies are in the range of 60 to 70%.

There are some small differences in the hardware trigger and tracking efficiencies between data and simulation. These differences are accounted for by weighting the simulation using data. The tracking-correction weight is obtained by multiplying the weights for each final-state particle, determined as a function of the particle momentum, transverse momentum, dipole magnet polarity and event charged-particle multiplicity [17]. The impact of this correction on the individual efficiencies is at the level of 3%.

The trigger efficiency correction follows the method described in ref. [18]. The total data sample for each decay mode is separated into two mutually exclusive subsamples. The first is composed of candidates that are triggered at the hardware level by one or more of the final state particles interacting in the hadronic calorimeter. The second is composed of candidates triggered only by particles in the rest of the event. The correction makes use of calibration data samples of $D^0 \to K^-\pi^+$ decays and affects differently these two subsamples. The correction factors are evaluated as a function of the DP position for each subsample and combined into a single efficiency correction map according to their proportions in data.

The final efficiency maps, obtained after the full selection and corrections described above, are shown in figure 2, for all decays, for *MagDown* polarity (the plots for *MagUp* are similar). The binning schemes used for each mode are introduced in these plots. The corresponding average efficiencies vary among the different decay modes from 2.7×10^{-4} (for $D_s^+ \to K^-K^+\pi^+$) to 7.0×10^{-4} (for $D^+ \to K^-K^+\pi^+$). The different lifetimes of the parent mesons and different PID criteria are the predominant contributions to this variation. The ratios between signal and normalisation channels are given in table 2. The impact of the different corrections (tracking, trigger and charged-particle multiplicity) applied to the efficiencies is below 1.5% for all ratios.

JHEP03(2019)176

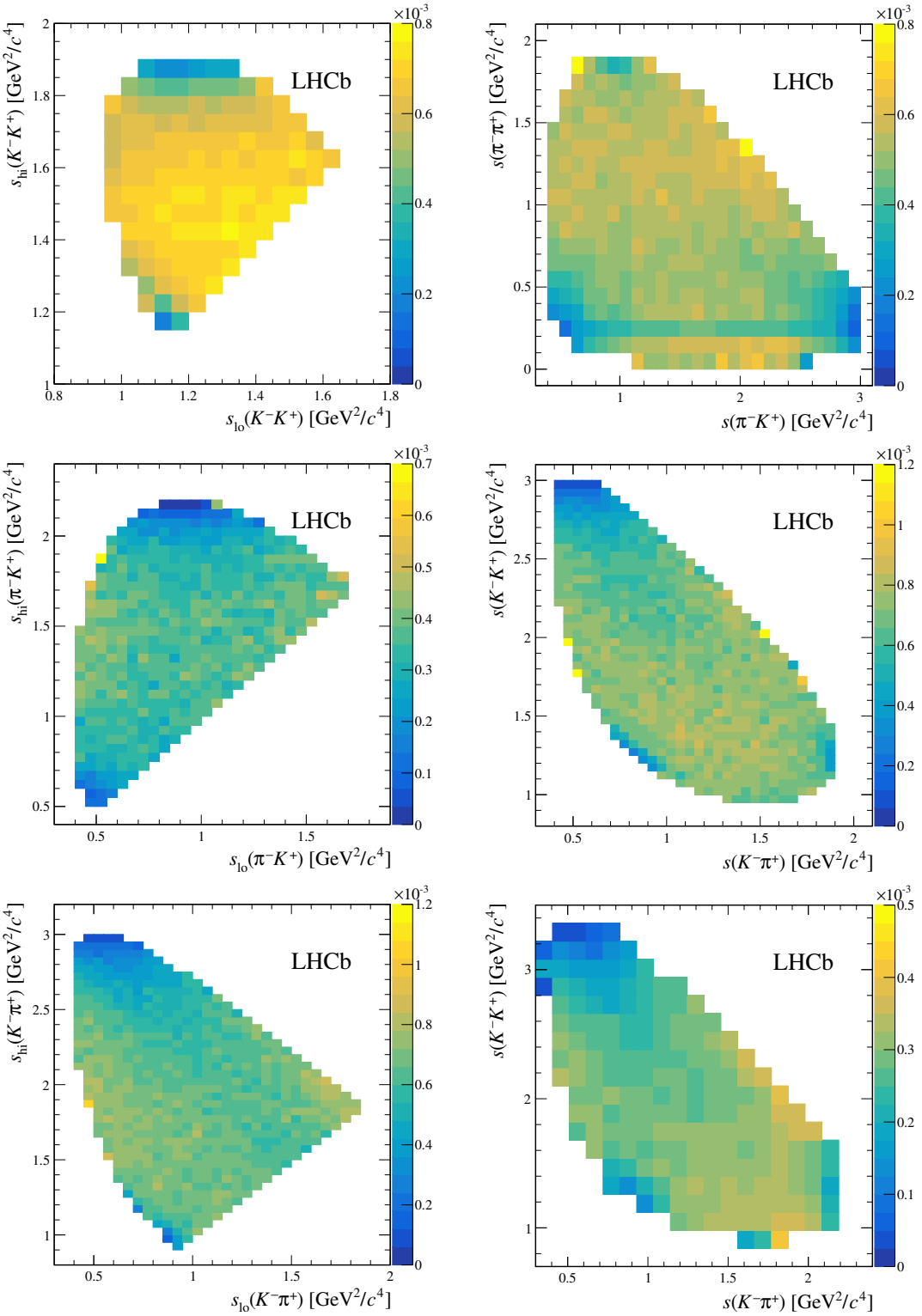

Figure 2. Efficiency maps for (top left) $D^+ \to K^-K^+K^+$, (top right) $D^+ \to \pi^-\pi^+K^+$, (middle left) $D_s^+ \to \pi^-K^+K^+$, (middle right) $D^+ \to K^-K^+\pi^+$, (bottom left) $D^+ \to K^-\pi^+\pi^+$ and (bottom right) $D_s^+ \to K^-K^+\pi^+$ decays with PID efficiency, tracking, multiplicity and hardware trigger efficiency corrections, for *MagDown* polarity.

JHEP03(2019)176

Ratio of efficiencies	*MagDown*	*MagUp*
$\varepsilon_{D^+\to K^-K^+K^+}/\varepsilon_{D^+\to K^-\pi^+\pi^+}$	1.0024 ± 0.0034	1.0077 ± 0.0033
$\varepsilon_{D^+\to\pi^-\pi^+K^+}/\varepsilon_{D^+\to K^-\pi^+\pi^+}$	0.958 ± 0.005	0.956 ± 0.005
$\varepsilon_{D_s^+\to\pi^-K^+K^+}/\varepsilon_{D_s^+\to K^-K^+\pi^+}$	1.242 ± 0.013	1.215 ± 0.014
$\varepsilon_{D^+\to K^-K^+\pi^+}/\varepsilon_{D^+\to K^-\pi^+\pi^+}$	1.096 ± 0.008	1.108 ± 0.009

Table 2. Ratios of average efficiencies for the full selection. The quoted uncertainty is due to the limited size of the simulated sample only (see section 7).

6 Determination of the yields

The yields of the signal and normalisation channels are determined by extended binned maximum-likelihood fits to the invariant-mass distribution of each sample independently. For each channel, the signal probability distribution function (PDF) is represented by a sum of a Gaussian function and two Crystal Ball (CB) [19] functions, while the background is modelled by an exponential function. The signal PDF is

$$\mathcal{P}_{\rm sig}(M) = f_{\rm G} \times {\rm G}(\mu, \sigma_{\rm G}) + (1 - f_{\rm G}) \times [f_{\rm CB} \times {\rm CB}_1(\mu, R_1\sigma_{\rm G}, \alpha_1, N_1) + (1 - f_{\rm CB}) \times {\rm CB}_2(\mu, R_2\sigma_{\rm G}, \alpha_2, N_2)] \,, \quad (6.1)$$

where μ and $\sigma_{\rm G}$ are the mean value and the width of the Gaussian function G. The two Crystal Ball functions, $\rm CB_1$ and $\rm CB_2$, have widths $R_1\sigma_{\rm G}$ and $R_2\sigma_{\rm G}$, and tail parameters α_1, N_1 and α_2, N_2. A common parameter, μ, describes the most probable mass value of the two Crystal Balls and the mean of the Gaussian function.

The fractions of each PDF component are $f_{\rm G}$ for the Gaussian function, $(1-f_{\rm G}) \times f_{\rm CB}$ for $\rm CB_1$ and $(1-f_{\rm G}) \times (1-f_{\rm CB})$ for $\rm CB_2$. The parameters α_i, N_i, R_i, $f_{\rm CB}$ and $f_{\rm G}$ defining the signal PDF are fixed to the values obtained from a fit to the simulation sample. The position of the signal mass peak presents a small dependence on the charge of the $D^+_{(s)}$ meson and on the magnet polarity. Therefore, the samples are divided into four subsamples to ensure a precise determination of the yields.

Due to the large size of the samples of CF channels $D^+ \to K^-\pi^+\pi^+$, $D_s^+ \to K^-K^+\pi^+$ and for the CS channel $D^+ \to K^-K^+\pi^+$, the convergence and goodness of the fit are sensitive to the momentum-dependent resolution of the $D^+_{(s)}$ candidate, making it difficult to fit these samples with a single set of parameters. For this reason, the $D^+ \to K^-\pi^+\pi^+$ and $D^+ \to K^-K^+\pi^+$ ($D_s^+ \to K^-K^+\pi^+$) samples are further divided into 50 (20) bins of $D^+_{(s)}$ momentum. The variation of $\sigma_{\rm G}$ over the momentum bins is of the order of 50%. For each magnet polarity, the total signal yield, shown in table 3, is the sum of the yields in the different subsets. For illustration purposes, the invariant-mass distribution for each of the DCS decay modes and for the CS channel are shown in figure 3 for the whole sample, summing also over the two magnet polarities, with the associated fit results superimposed. The mass distributions for the CF normalisation modes are shown in figure 4.

The observed signal yields in bins of the DP, $N_i^{\rm obs}$ in eq. (3.2), are determined using the *sPlot* technique [20]. For each data subset, the signal and background *sWeights* are

JHEP03(2019)176

	Yields [$\times 10^3$]		
Channel	*MagDown*	*MagUp*	Total
$D^+ \to K^-K^+K^+$	67.61 ± 0.33	66.69 ± 0.33	134.30 ± 0.47
$D^+ \to \pi^-\pi^+K^+$	401.2 ± 1.0	393.7 ± 1.0	794.9 ± 1.4
$D_s^+ \to \pi^-K^+K^+$	33.7 ± 0.4	33.6 ± 0.4	67.2 ± 0.5
$D^+ \to K^-K^+\pi^+$	$11\,657 \pm 4$	$11\,482 \pm 4$	$23\,139 \pm 5$
$D^+ \to K^-\pi^+\pi^+$ (†)	$103\,282 \pm 10$	$101\,008 \pm 10$	$204\,290 \pm 14$
$D^+ \to K^-\pi^+\pi^+$ (††)	$80\,197 \pm 10$	$78\,530 \pm 10$	$158\,727 \pm 13$
$D_s^+ \to K^-K^+\pi^+$	$11\,629 \pm 4$	$11\,414 \pm 4$	$23\,044 \pm 5$

Table 3. Observed yields for signal and normalisation modes with statistical uncertainties. The entry for the decay $D^+ \to K^-\pi^+\pi^{+(\dagger)}$ corresponds to the yields obtained from the fit to $D^+ \to K^-\pi^+\pi^+$ sample with cuts optimised for the $D^+ \to K^-K^+K^+$ and $D^+ \to K^-K^+\pi^+$ selections. The entry for the decay $D^+ \to K^-\pi^+\pi^{+(\dagger\dagger)}$ is for fits to $D^+ \to K^-\pi^+\pi^+$ samples with cuts optimised for the $D^+ \to \pi^-\pi^+K^+$ selection.

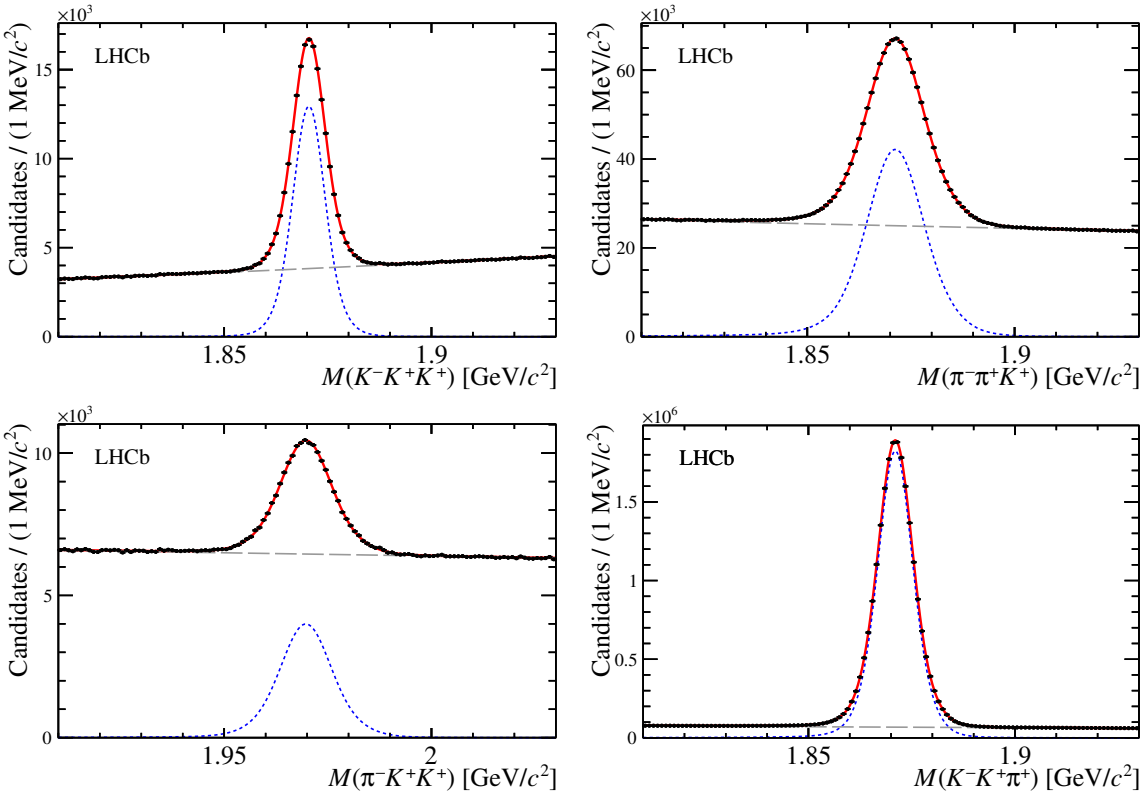

Figure 3. Invariant-mass distributions of (top left) $D^+ \to K^-K^+K^+$, (top right) $D^+ \to \pi^-\pi^+K^+$, (bottom left) $D_s^+ \to \pi^-K^+K^+$ and (bottom right) $D^+ \to K^-K^+\pi^+$ with the corresponding fit result superimposed (red solid line). The blue dotted line corresponds to the signal PDF and the dashed grey line shows the background PDF.

JHEP03(2019)176

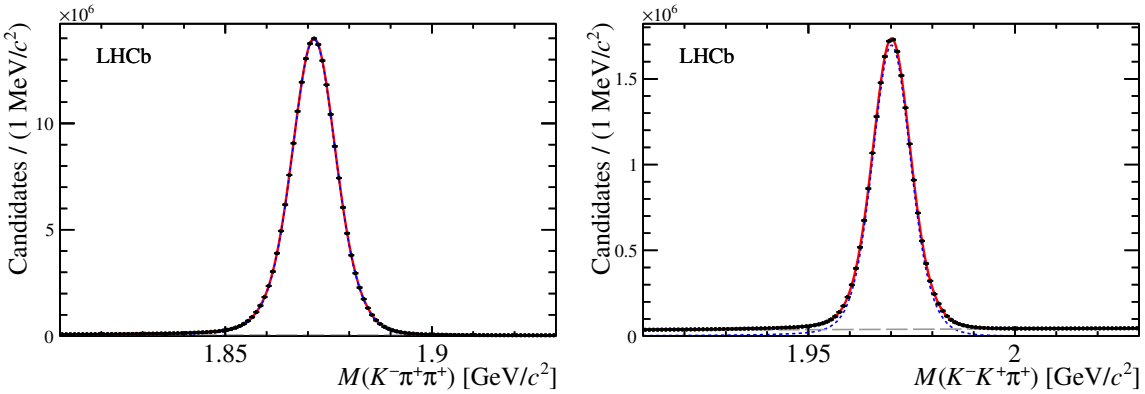

Figure 4. Invariant-mass distributions of candidates of the normalisation modes (left) $D^+ \to K^-\pi^+\pi^+$ and (right) $D_s^+ \to K^-K^+\pi^+$ with the corresponding fit result superimposed (red solid line). The blue dotted line corresponds to the signal PDF and the dashed grey line shows the background PDF.

	Produced yields [$\times 10^7$]	
Decay	*MagDown*	*MagUp*
$D^+ \to K^-K^+K^+$	10.52 ± 0.06	10.54 ± 0.06
$D^+ \to \pi^-\pi^+K^+$	84.2 ± 0.4	84.4 ± 0.4
$D_s^+ \to \pi^-K^+K^+$	9.85 ± 0.15	10.04 ± 0.17
$D^+ \to K^-K^+\pi^+$	1659 ± 12	1651 ± 13
$D^+ \to K^-\pi^+\pi^+(\dagger)$	16103 ± 40	16092 ± 40
$D^+ \to K^-\pi^+\pi^+(\dagger\dagger)$	16130 ± 50	16101 ± 50
$D_s^+ \to K^-K^+\pi^+$	4221 ± 34	4150 ± 33

Table 4. Produced yields for each decay mode with statistical uncertainties, shown separately for *MagDown* and *MagUp* samples. The numbers given for the decay $D^+ \to K^-\pi^+\pi^{+(\dagger)}$ correspond to the sample with cuts optimised for the $D^+ \to K^-K^+K^+$ and $D^+ \to K^-K^+\pi^+$ and those for the decay $D^+ \to K^-\pi^+\pi^{+(\dagger\dagger)}$ to the sample with cuts optimised for the $D^+ \to \pi^-\pi^+K^+$ selection.

obtained from the maximum-likelihood fit, and the former are used to compute the number of signal candidates in each bin of the phase space for each data subset. No significant correlation between the $D_{(s)}^+$ candidate mass and position in the DP is observed. The DP with the total signal yields for all decays (merging $D_{(s)}^+$ and $D_{(s)}^-$, *MagDown* and *MagUp* subsets) are shown in figure 5.

With the yields of observed candidates and the efficiencies obtained in bins of the DP for signal and normalisation modes, the total yields produced in the pp collisions are evaluated using eq. (3.2). These numbers are listed in table 4, separately for the *MagDown* and *MagUp* samples and can then be used for the determination of the different ratios of branching fractions.

JHEP03(2019)176

7 Systematic uncertainties

Due to the similar decay topologies and selections applied to signal and normalisation channels within independent data subsets, many systematic uncertainties related to the final state factorise and cancel in the ratio of signal to normalisation yields and efficiencies.

The systematic uncertainties due to the limited size of the simulation samples are determined using pseudoexperiments. The number of generated events in each pseudoexperiment is obtained randomly in bins of the DP according to a Poisson distribution and corrected by the nominal efficiency and correction maps due to PID, tracking and trigger. The uncertainties of the signal and normalisation efficiencies are taken as the Gaussian width of the resulting distributions of average efficiencies. The mean value of these distributions are compatible with the nominal values. The resulting uncertainties of the ratios of efficiencies are given in table 2 and the corresponding relative systematic uncertainties are given in table 5.

In order to estimate the uncertainties on the ratios of effective efficiencies arising from the limited size of the calibration samples used to determine the PID efficiency and the tracking and trigger corrections, 100 tables are generated, with efficiencies or corrections fluctuating according to Gaussian functions centred at the nominal value and with width equal to their nominal uncertainties. For each generated table, the DP map of efficiencies are re-evaluated for signal and normalisation channels using the same procedure as the one used for the determination of the nominal efficiency maps. The distribution of the efficiency ratio is fitted with a Gaussian function, whose width is taken as systematic uncertainty.

An additional systematic uncertainty is assigned to the ratios of tracking efficiencies when signal and normalisation decay modes have a different number of kaons and pions in the final state. The fractions of kaons and pions which cannot be reconstructed due to hadronic interactions that occur before the last tracking station are estimated using a simulated sample of $D^+ \to K^-\pi^+\pi^+$ decays. Assuming a 10% uncertainty on the description of the detector material [17], per-track uncertainties on the efficiency of kaons and pions of (1.432±0.015)% and (1.702±0.011)%, respectively, are obtained. The residual uncertainties due to the different interactions of particles with opposite charge with the detector material are estimated to be negligible when compared to the uncertainty due to the limited size of the calibration samples, since the final branching-fraction ratios are averaged over particle charge and magnet polarity. This is the most important source of systematic uncertainty for the $\mathcal{B}(D^+ \to K^-K^+K^+)/\mathcal{B}(D^+ \to K^-\pi^+\pi^+)$ measurement.

The systematic uncertainty due to the fit model is estimated using an alternative parametrisation for the signal based on the sum of two CB functions with a common mean. The observed yields obtained with this model are used to measure the branching-fraction ratios with the same procedure as for the nominal evaluation and the difference between the two results is assigned as systematic uncertainty.

The effect of residual charm contamination is studied. The stringent PID requirements are chosen to suppress the charm backgrounds to minimal levels, so that any remaining contribution does not affect the signal yields, either because the number of candidates is very low or because its shape is broad enough to be absorbed in the yield of the combinatorial

JHEP03(2019)176

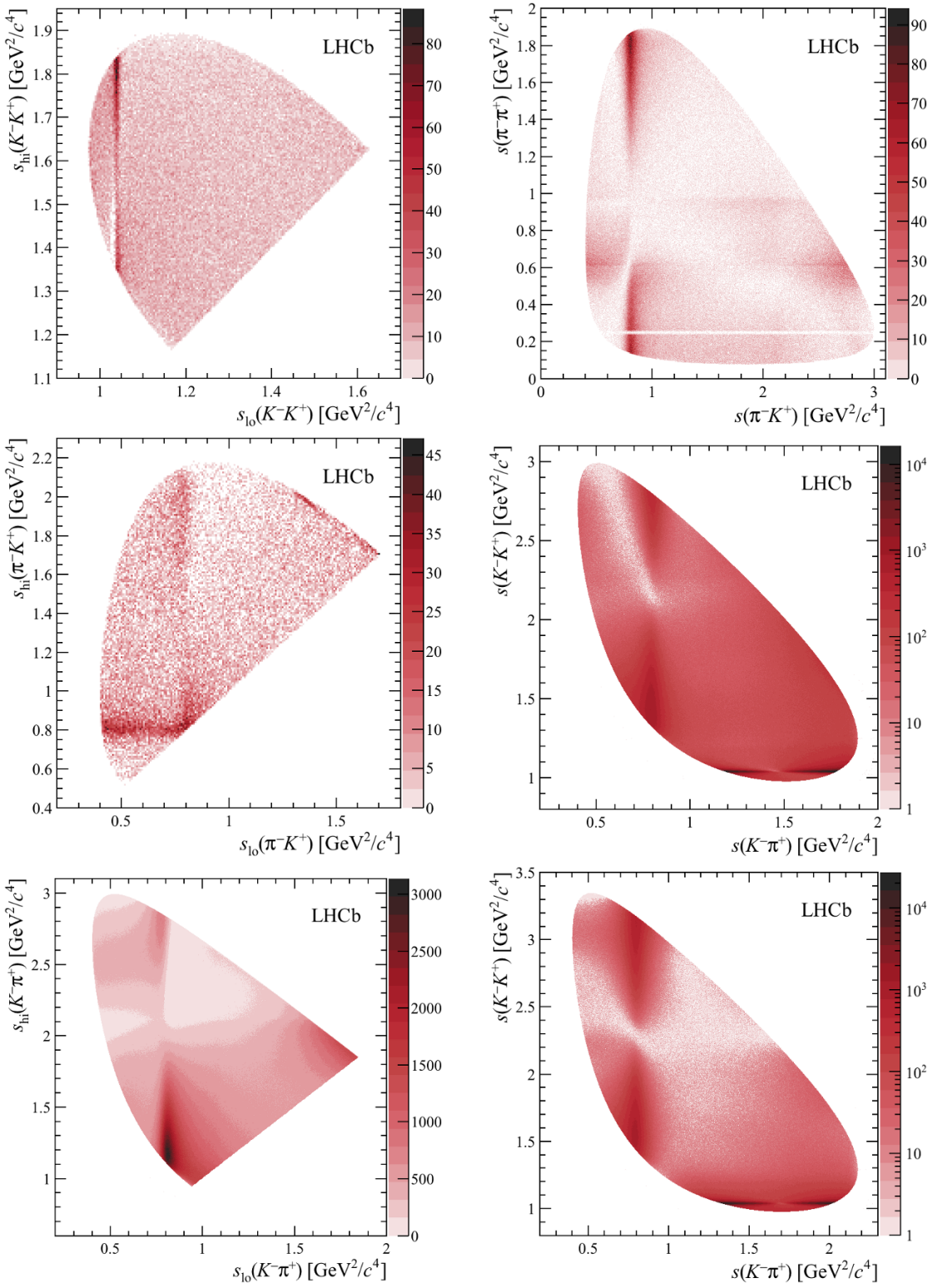

Figure 5. Dalitz plots of the (top left) $D^+ \to K^-K^+K^+$, (top right) $D^+ \to \pi^-\pi^+K^+$, where the K^0_S veto can be seen, (middle left) $D^+_s \to \pi^-K^+K^+$, (middle right) $D^+ \to K^-K^+\pi^+$, (bottom left) $D^+ \to K^-\pi^+\pi^+$ and (bottom right) $D^+_s \to K^-K^+\pi^+$ decays, with signal weights from *sPlot*. A logarithmic scale is used for the $D^+ \to K^-K^+\pi^+$ and $D^+_s \to K^-K^+\pi^+$ channels.

JHEP03(2019)176

Source	$\frac{\mathcal{B}(D^+\to K^-K^+K^+)}{\mathcal{B}(D^+\to K^-\pi^+\pi^+)}$	$\frac{\mathcal{B}(D^+\to \pi^-\pi^+K^+)}{\mathcal{B}(D^+\to K^-\pi^+\pi^+)}$	$\frac{\mathcal{B}(D_s^+\to \pi^-K^+K^+)}{\mathcal{B}(D_s^+\to K^-K^+\pi^+)}$	$\frac{\mathcal{B}(D^+\to K^-K^+\pi^+)}{\mathcal{B}(D^+\to K^-\pi^+\pi^+)}$
MagDown				
Size of simulation	0.34	0.47	1.0	0.75
PID	0.022	0.019	0.022	0.013
Tracking	0.22	0.069	0.079	0.11
Trigger corr.	0.011	0.0025	0.0050	0.0057
Mat. description	0.53	—	—	0.27
Fit Model	0.14	0.03	0.64	0.06
Sec. decays	0.18	0.25	0.31	0.11
DP Binning	0.09	0.05	0.30	0.13
Total syst.	0.72	0.54	1.3	0.82
Statistical	0.54	0.25	1.4	0.03
MagUp				
Size of simulation	0.32	0.52	1.2	0.81
PID	0.030	0.020	0.023	0.021
Tracking	0.22	0.070	0.080	0.10
Trigger corr.	0.011	0.0024	0.0057	0.0060
Mat. description	0.53	—	—	0.27
Fit Model	0.13	0.07	0.54	0.06
Sec. decays	0.18	0.24	0.38	0.09
DP Binning	0.11	0.03	0.07	0.28
Total syst.	0.71	0.58	1.3	0.91
Statistical	0.54	0.25	1.4	0.03

Table 5. Relative systematic uncertainties for the *MagDown* and *MagUp* results (in %). The statistical uncertainties are also given for comparison.

background. This assumption is tested by explicitly estimating the residual contaminations and their shapes from data and simulation, and including them in the mass fits. No significant effects are found for any of the signal modes. The impact of the mass vetoes used to reject the Λ_c^+ contamination is studied by further enlarging the mass-veto window by $5\,\mathrm{MeV}/c^2$ for all channels. No significant deviation is observed in any of the final results and therefore no systematic uncertainty is assigned.

The effect of a potential contamination from decays of $D^+_{(s)}$ from b-hadron decays, which could be different for signal and normalisation samples, is investigated by tightening the requirement on χ^2_{IP} to two alternative values and measuring the ratios of branching fractions. The largest deviation from the nominal value is assigned as systematic uncertainty.

The systematic uncertainty due to the choice of DP binning scheme is evaluated as the deviation of the ratio of produced yields obtained with alternative binning schemes from

JHEP03(2019)176

Channel	*MagDown* ($\times 10^{-3}$)
$\mathcal{B}(D^+ \to K^-K^+K^+)/\mathcal{B}(D^+ \to K^-\pi^+\pi^+)$	$0.653 \pm 0.004 \pm 0.005$
$\mathcal{B}(D^+ \to \pi^-\pi^+K^+)/\mathcal{B}(D^+ \to K^-\pi^+\pi^+)$	$5.220 \pm 0.013 \pm 0.028$
$\mathcal{B}(D_s^+ \to \pi^-K^+K^+)/\mathcal{B}(D_s^+ \to K^-K^+\pi^+)$	$2.333 \pm 0.033 \pm 0.030$
$\mathcal{B}(D^+ \to K^-K^+\pi^+)/\mathcal{B}(D^+ \to K^-\pi^+\pi^+)$	$103.00 \pm 0.03 \pm 0.85$
Channel	*MagUp* ($\times 10^{-3}$)
$\mathcal{B}(D^+ \to K^-K^+K^+)/\mathcal{B}(D^+ \to K^-\pi^+\pi^+)$	$0.655 \pm 0.004 \pm 0.005$
$\mathcal{B}(D^+ \to \pi^-\pi^+K^+)/\mathcal{B}(D^+ \to K^-\pi^+\pi^+)$	$5.244 \pm 0.013 \pm 0.030$
$\mathcal{B}(D_s^+ \to \pi^-K^+K^+)/\mathcal{B}(D_s^+ \to K^-K^+\pi^+)$	$2.419 \pm 0.035 \pm 0.032$
$\mathcal{B}(D^+ \to K^-K^+\pi^+)/\mathcal{B}(D^+ \to K^-\pi^+\pi^+)$	$102.59 \pm 0.03 \pm 0.93$

Table 6. Ratios of branching fractions, shown separately for *MagDown* and *MagUp* samples. The first uncertainty is statistical and the second is systematic.

that obtained with the nominal binning schemes. These binning schemes are defined by changing the nominal number of bins by ± 1, ± 2 and ± 4 units in each DP axis.

The systematic uncertainties due to the different sources considered in this analysis are summarised in table 5, separately for the *MagDown* and *MagUp* results. Except for the $\mathcal{B}(D^+ \to K^-K^+K^+)/\mathcal{B}(D^+ \to K^-\pi^+\pi^+)$ measurement, the most important source of systematic uncertainty is the limited size of the simulation samples. However, the only result with total uncertainty dominated by this contribution is the branching-fraction ratio of the CS decay $D^+ \to K^-K^+\pi^+$.

The ratios of branching fractions obtained with data taken with the two magnet polarities are shown in table 6, with statistical and systematic uncertainties. For each decay mode the two results are compatible and no additional systematic uncertainty is assigned to the effect of detector asymmetry.

8 Results

Final ratios of branching fractions are obtained by combining the two measurements shown in table 6, accounting for 100% correlation [21] between the systematic uncertainties due to the material description in the simulation, fit model, contamination from secondary decays and DP binning. For the doubly Cabibbo-suppressed channels, the results are

$$\frac{\mathcal{B}(D^+ \to K^-K^+K^+)}{\mathcal{B}(D^+ \to K^-\pi^+\pi^+)} = (6.541 \pm 0.025 \pm 0.042) \times 10^{-4},$$
$$\frac{\mathcal{B}(D^+ \to \pi^-\pi^+K^+)}{\mathcal{B}(D^+ \to K^-\pi^+\pi^+)} = (5.231 \pm 0.009 \pm 0.023) \times 10^{-3},$$
$$\frac{\mathcal{B}(D_s^+ \to \pi^-K^+K^+)}{\mathcal{B}(D_s^+ \to K^-K^+\pi^+)} = (2.372 \pm 0.024 \pm 0.025) \times 10^{-3},$$

JHEP03(2019)176

where the first uncertainty is statistical and the second systematic. These values are consistent with the current world averages, being compatible at the 1.4σ, 2.4σ and 0.2σ levels, respectively.

In addition, the result for the Cabibbo-suppressed mode $D^+ \to K^-K^+\pi^+$ is

$$\frac{\mathcal{B}(D^+ \to K^-K^+\pi^+)}{\mathcal{B}(D^+ \to K^-\pi^+\pi^+)} = (10.282 \pm 0.002 \pm 0.068) \times 10^{-2},$$

where again the first uncertainties are statistical and the second systematic. It is in agreement with the world average [3] at the 1.6σ level, improving the precision by a factor 2.6.

The ratios of branching fractions are combined with the world-average values [3] of the branching fractions of the CF decays $D^+ \to K^-\pi^+\pi^+$ $(8.98 \pm 0.28)\%$ and $D_s^+ \to K^-K^+\pi^+$ $(5.45 \pm 0.17)\%$ to compute the branching fractions of the DCS modes

$$\begin{aligned}
\mathcal{B}(D^+ \to K^-K^+K^+) &= (5.87 \pm 0.02 \pm 0.04 \pm 0.18) \times 10^{-5}, \\
\mathcal{B}(D^+ \to \pi^-\pi^+K^+) &= (4.70 \pm 0.01 \pm 0.02 \pm 0.15) \times 10^{-4}, \\
\mathcal{B}(D_s^+ \to \pi^-K^+K^+) &= (1.293 \pm 0.013 \pm 0.014 \pm 0.040) \times 10^{-4},
\end{aligned}$$

and of the CS mode

$$\mathcal{B}(D^+ \to K^-K^+\pi^+) = (9.233 \pm 0.002 \pm 0.061 \pm 0.288) \times 10^{-3},$$

where the uncertainties are statistical, systematic and due to the uncertainty of the normalisation channel, respectively. Altogether, these represent the best measurements up to date.

Acknowledgments

We express our gratitude to our colleagues in the CERN accelerator departments for the excellent performance of the LHC. We thank the technical and administrative staff at the LHCb institutes. We acknowledge support from CERN and from the national agencies: CAPES, CNPq, FAPERJ and FINEP (Brazil); MOST and NSFC (China); CNRS/IN2P3 (France); BMBF, DFG and MPG (Germany); INFN (Italy); NWO (Netherlands); MNiSW and NCN (Poland); MEN/IFA (Romania); MSHE (Russia); MinECo (Spain); SNSF and SER (Switzerland); NASU (Ukraine); STFC (United Kingdom); NSF (U.S.A.). We acknowledge the computing resources that are provided by CERN, IN2P3 (France), KIT and DESY (Germany), INFN (Italy), SURF (Netherlands), PIC (Spain), GridPP (United Kingdom), RRCKI and Yandex LLC (Russia), CSCS (Switzerland), IFIN-HH (Romania), CBPF (Brazil), PL-GRID (Poland) and OSC (U.S.A.). We are indebted to the communities behind the multiple open-source software packages on which we depend. Individual groups or members have received support from AvH Foundation (Germany); EPLANET, Marie Skłodowska-Curie Actions and ERC (European Union); ANR, Labex P2IO and OCEVU, and Région Auvergne-Rhône-Alpes (France); Key Research Program of Frontier Sciences of CAS, CAS PIFI, and the Thousand Talents Program (China); RFBR, RSF and Yandex LLC (Russia); GVA, XuntaGal and GENCAT (Spain); the Royal Society and the Leverhulme Trust (United Kingdom); Laboratory Directed Research and Development program of LANL (U.S.A.).

JHEP03(2019)176

References

[1] B. Bhattacharya and J.L. Rosner, *Flavor symmetry and decays of charmed mesons to pairs of light pseudoscalars*, *Phys. Rev.* **D 77** (2008) 114020 [arXiv:0803.2385] [INSPIRE].

[2] L.-L. Chau, *Quark Mixing in Weak Interactions*, *Phys. Rept.* **95** (1983) 1 [INSPIRE].

[3] Particle Data Group collaboration, *Review of Particle Physics*, *Phys. Rev.* **D 98** (2018) 030001 [INSPIRE] and online at http://pdg.lbl.gov/.

[4] FOCUS collaboration, *Measurement of the D^+ and D_s^+ Decays into $K^+K^-K^+$*, *Phys. Lett.* **B 541** (2002) 227 [hep-ex/0206049] [INSPIRE].

[5] LHCb collaboration, *The LHCb Detector at the LHC*, 2008 *JINST* **3** S08005 [INSPIRE].

[6] LHCb collaboration, *LHCb Detector Performance*, *Int. J. Mod. Phys.* **A 30** (2015) 1530022 [arXiv:1412.6352] [INSPIRE].

[7] LHCb RICH Group collaboration, *Performance of the LHCb RICH detector at the LHC*, *Eur. Phys. J.* **C 73** (2013) 2431 [arXiv:1211.6759] [INSPIRE].

[8] R. Aaij et al., *The LHCb Trigger and its Performance in 2011*, 2013 *JINST* **8** P04022 [arXiv:1211.3055] [INSPIRE].

[9] T. Sjöstrand, S. Mrenna and P.Z. Skands, *PYTHIA 6.4 Physics and Manual*, *JHEP* **05** (2006) 026 [hep-ph/0603175] [INSPIRE].

[10] LHCb collaboration, *Handling of the generation of primary events in Gauss, the LHCb simulation framework*, *J. Phys. Conf. Ser.* **331** (2011) 032047 [INSPIRE].

[11] D.J. Lange, *The EvtGen particle decay simulation package*, *Nucl. Instrum. Meth.* **A 462** (2001) 152 [INSPIRE].

[12] P. Golonka and Z. Was, *PHOTOS Monte Carlo: A Precision tool for QED corrections in Z and W decays*, *Eur. Phys. J.* **C 45** (2006) 97 [hep-ph/0506026] [INSPIRE].

[13] J. Allison et al., *Geant4 developments and applications*, *IEEE Trans. Nucl. Sci.* **53** (2006) 270 [INSPIRE].

[14] M. Clemencic et al., *The LHCb simulation application, Gauss: Design, evolution and experience*, *J. Phys. Conf. Ser.* **331** (2011) 032023 [INSPIRE].

[15] R.H. Dalitz, *On the analysis of τ-meson data and the nature of the τ-meson*, *Phil. Mag. Ser.* **44** (1953) 1068 [INSPIRE].

[16] L. Anderlini et al., *The PIDCalib package*, LHCb-PUB-2016-021.

[17] LHCb collaboration, *Measurement of the track reconstruction efficiency at LHCb*, 2015 *JINST* **10** P02007 [arXiv:1408.1251] [INSPIRE].

[18] LHCb collaboration, *Dalitz plot analysis of $B_s^0 \to \bar{D}^0 K^- \pi^+$ decays*, *Phys. Rev.* **D 90** (2014) 072003 [arXiv:1407.7712] [INSPIRE].

JHEP03(2019)176

[19] T. Skwarnicki, *A study of the radiative CASCADE transitions between the Upsilon-prime and Upsilon resonances*, Ph.D. Thesis, Institute of Nuclear Physics, Krakow Poland (1986) [DESY-F31-86-02] [INSPIRE].

[20] M. Pivk and F.R. Le Diberder, *SPlot: A Statistical tool to unfold data distributions*, *Nucl. Instrum. Meth.* **A 555** (2005) 356 [physics/0402083] [INSPIRE].

[21] R. Nisius, *On the combination of correlated estimates of a physics observable*, *Eur. Phys. J.* **C 74** (2014) 3004 [arXiv:1402.4016] [INSPIRE].

JHEP03(2019)176

The LHCb collaboration

R. Aaij[27], C. Abellán Beteta[44], B. Adeva[41], M. Adinolfi[48], C.A. Aidala[76], Z. Ajaltouni[5], S. Akar[59], P. Albicocco[18], J. Albrecht[10], F. Alessio[42], M. Alexander[53], A. Alfonso Albero[40], G. Alkhazov[33], P. Alvarez Cartelle[55], A.A. Alves Jr[41], S. Amato[2], S. Amerio[23], Y. Amhis[7], L. An[3], L. Anderlini[17], G. Andreassi[43], M. Andreotti[16], J.E. Andrews[60], R.B. Appleby[56], F. Archilli[27], P. d'Argent[12], J. Arnau Romeu[6], A. Artamonov[39], M. Artuso[61], K. Arzymatov[37], E. Aslanides[6], M. Atzeni[44], B. Audurier[22], S. Bachmann[12], J.J. Back[50], S. Baker[55], V. Balagura[7,b], W. Baldini[16], A. Baranov[37], R.J. Barlow[56], S. Barsuk[7], W. Barter[56], F. Baryshnikov[72], V. Batozskaya[31], B. Batsukh[61], A. Battig[10], V. Battista[43], A. Bay[43], J. Beddow[53], F. Bedeschi[24], I. Bediaga[1], A. Beiter[61], L.J. Bel[27], S. Belin[22], N. Beliy[64], V. Bellee[43], N. Belloli[20,i], K. Belous[39], I. Belyaev[34], E. Ben-Haim[8], G. Bencivenni[18], S. Benson[27], S. Beranek[9], A. Berezhnoy[35], R. Bernet[44], D. Berninghoff[12], E. Bertholet[8], A. Bertolin[23], C. Betancourt[44], F. Betti[15,42], M.O. Bettler[49], M. van Beuzekom[27], Ia. Bezshyiko[44], S. Bhasin[48], J. Bhom[29], S. Bifani[47], P. Billoir[8], A. Birnkraut[10], A. Bizzeti[17,u], M. Bjørn[57], M.P. Blago[42], T. Blake[50], F. Blanc[43], S. Blusk[61], D. Bobulska[53], V. Bocci[26], O. Boente Garcia[41], T. Boettcher[58], A. Bondar[38,w], N. Bondar[33], S. Borghi[56,42], M. Borisyak[37], M. Borsato[41], F. Bossu[7], M. Boubdir[9], T.J.V. Bowcock[54], C. Bozzi[16,42], S. Braun[12], M. Brodski[42], J. Brodzicka[29], A. Brossa Gonzalo[50], D. Brundu[22,42], E. Buchanan[48], A. Buonaura[44], C. Burr[56], A. Bursche[22], J. Buytaert[42], W. Byczynski[42], S. Cadeddu[22], H. Cai[66], R. Calabrese[16,g], R. Calladine[47], M. Calvi[20,i], M. Calvo Gomez[40,m], A. Camboni[40,m], P. Campana[18], D.H. Campora Perez[42], L. Capriotti[15], A. Carbone[15,e], G. Carboni[25], R. Cardinale[19,h], A. Cardini[22], P. Carniti[20,i], L. Carson[52], K. Carvalho Akiba[2], G. Casse[54], L. Cassina[20], M. Cattaneo[42], G. Cavallero[19], R. Cenci[24,p], D. Chamont[7], M.G. Chapman[48], M. Charles[8], Ph. Charpentier[42], G. Chatzikonstantinidis[47], M. Chefdeville[4], V. Chekalina[37], C. Chen[3], S. Chen[22], S.-G. Chitic[42], V. Chobanova[41], M. Chrzaszcz[42], A. Chubykin[33], P. Ciambrone[18], X. Cid Vidal[41], G. Ciezarek[42], P.E.L. Clarke[52], M. Clemencic[42], H.V. Cliff[49], J. Closier[42], V. Coco[42], J.A.B. Coelho[7], J. Cogan[6], E. Cogneras[5], L. Cojocariu[32], P. Collins[42], T. Colombo[42], A. Comerma-Montells[12], A. Contu[22], G. Coombs[42], S. Coquereau[40], G. Corti[42], M. Corvo[16,g], C.M. Costa Sobral[50], B. Couturier[42], G.A. Cowan[52], D.C. Craik[58], A. Crocombe[50], M. Cruz Torres[1], R. Currie[52], C. D'Ambrosio[42], F. Da Cunha Marinho[2], C.L. Da Silva[77], E. Dall'Occo[27], J. Dalseno[48], A. Danilina[34], A. Davis[3], O. De Aguiar Francisco[42], K. De Bruyn[42], S. De Capua[56], M. De Cian[43], J.M. De Miranda[1], L. De Paula[2], M. De Serio[14,d], P. De Simone[18], C.T. Dean[53], D. Decamp[4], L. Del Buono[8], B. Delaney[49], H.-P. Dembinski[11], M. Demmer[10], A. Dendek[30], D. Derkach[37], O. Deschamps[5], F. Desse[7], F. Dettori[54], B. Dey[67], A. Di Canto[42], P. Di Nezza[18], S. Didenko[72], H. Dijkstra[42], F. Dordei[42], M. Dorigo[42,x], A. Dosil Suárez[41], L. Douglas[53], A. Dovbnya[45], K. Dreimanis[54], L. Dufour[27], G. Dujany[8], P. Durante[42], J.M. Durham[77], D. Dutta[56], R. Dzhelyadin[39], M. Dziewiecki[12], A. Dziurda[29], A. Dzyuba[33], S. Easo[51], U. Egede[55], V. Egorychev[34], S. Eidelman[38,w], S. Eisenhardt[52], U. Eitschberger[10], R. Ekelhof[10], L. Eklund[53], S. Ely[61], A. Ene[32], S. Escher[9], S. Esen[27], T. Evans[59], A. Falabella[15], N. Farley[47], S. Farry[54], D. Fazzini[20,42,i], L. Federici[25], P. Fernandez Declara[42], A. Fernandez Prieto[41], F. Ferrari[15], L. Ferreira Lopes[43], F. Ferreira Rodrigues[2], M. Ferro-Luzzi[42], S. Filippov[36], R.A. Fini[14], M. Fiorini[16,g], M. Firlej[30], C. Fitzpatrick[43], T. Fiutowski[30], F. Fleuret[7,b], M. Fontana[42], F. Fontanelli[19,h], R. Forty[42], V. Franco Lima[54], M. Frank[42], C. Frei[42], J. Fu[21,q], W. Funk[42], C. Färber[42], M. Féo Pereira Rivello Carvalho[27], E. Gabriel[52], A. Gallas Torreira[41], D. Galli[15,e], S. Gallorini[23], S. Gambetta[52], Y. Gan[3], M. Gandelman[2], P. Gandini[21], Y. Gao[3], L.M. Garcia Martin[75], B. Garcia Plana[41], J. García Pardiñas[44], J. Garra Tico[49], L. Garrido[40], D. Gascon[40], C. Gaspar[42], L. Gavardi[10], G. Gazzoni[5], D. Gerick[12], E. Gersabeck[56], M. Gersabeck[56],

JHEP03(2019)176

T. Gershon[50], D. Gerstel[6], Ph. Ghez[4], S. Gianì[43], V. Gibson[49], O.G. Girard[43], L. Giubega[32], K. Gizdov[52], V.V. Gligorov[8], D. Golubkov[34], A. Golutvin[55,72], A. Gomes[1,a], I.V. Gorelov[35], C. Gotti[20,i], E. Govorkova[27], J.P. Grabowski[12], R. Graciani Diaz[40], L.A. Granado Cardoso[42], E. Graugés[40], E. Graverini[44], G. Graziani[17], A. Grecu[32], R. Greim[27], P. Griffith[22], L. Grillo[56], L. Gruber[42], B.R. Gruberg Cazon[57], O. Grünberg[69], C. Gu[3], E. Gushchin[36], A. Guth[9], Yu. Guz[39,42], T. Gys[42], C. Göbel[63], T. Hadavizadeh[57], C. Hadjivasiliou[5], G. Haefeli[43], C. Haen[42], S.C. Haines[49], B. Hamilton[60], X. Han[12], T.H. Hancock[57], S. Hansmann-Menzemer[12], N. Harnew[57], S.T. Harnew[48], T. Harrison[54], C. Hasse[42], M. Hatch[42], J. He[64], M. Hecker[55], K. Heinicke[10], A. Heister[10], K. Hennessy[54], L. Henry[75], E. van Herwijnen[42], J. Heuel[9], M. Heß[69], A. Hicheur[62], R. Hidalgo Charman[56], D. Hill[57], M. Hilton[56], P.H. Hopchev[43], W. Hu[67], W. Huang[64], Z.C. Huard[59], W. Hulsbergen[27], T. Humair[55], M. Hushchyn[37], D. Hutchcroft[54], D. Hynds[27], P. Ibis[10], M. Idzik[30], P. Ilten[47], K. Ivshin[33], R. Jacobsson[42], J. Jalocha[57], E. Jans[27], A. Jawahery[60], F. Jiang[3], M. John[57], D. Johnson[42], C.R. Jones[49], C. Joram[42], B. Jost[42], N. Jurik[57], S. Kandybei[45], M. Karacson[42], J.M. Kariuki[48], S. Karodia[53], N. Kazeev[37], M. Kecke[12], F. Keizer[49], M. Kelsey[61], M. Kenzie[49], T. Ketel[28], E. Khairullin[37], B. Khanji[42], C. Khurewathanakul[43], K.E. Kim[61], T. Kirn[9], S. Klaver[18], K. Klimaszewski[31], T. Klimkovich[11], S. Koliiev[46], M. Kolpin[12], R. Kopecna[12], P. Koppenburg[27], I. Kostiuk[27], S. Kotriakhova[33], M. Kozeiha[5], L. Kravchuk[36], M. Kreps[50], F. Kress[55], P. Krokovny[38,w], W. Krupa[30], W. Krzemien[31], W. Kucewicz[29,l], M. Kucharczyk[29], V. Kudryavtsev[38,w], A.K. Kuonen[43], T. Kvaratskheliya[34,42], D. Lacarrere[42], G. Lafferty[56], A. Lai[22], D. Lancierini[44], G. Lanfranchi[18], C. Langenbruch[9], T. Latham[50], C. Lazzeroni[47], R. Le Gac[6], A. Leflat[35], J. Lefrançois[7], R. Lefèvre[5], F. Lemaitre[42], O. Leroy[6], T. Lesiak[29], B. Leverington[12], P.-R. Li[64], T. Li[3], Z. Li[61], X. Liang[61], T. Likhomanenko[71], R. Lindner[42], F. Lionetto[44], V. Lisovskyi[7], G. Liu[65], X. Liu[3], D. Loh[50], A. Loi[22], I. Longstaff[53], J.H. Lopes[2], G.H. Lovell[49], D. Lucchesi[23,o], M. Lucio Martinez[41], A. Lupato[23], E. Luppi[16,g], O. Lupton[42], A. Lusiani[24], X. Lyu[64], F. Machefert[7], F. Maciuc[32], V. Macko[43], P. Mackowiak[10], S. Maddrell-Mander[48], O. Maev[33,42], K. Maguire[56], D. Maisuzenko[33], M.W. Majewski[30], S. Malde[57], B. Malecki[29], A. Malinin[71], T. Maltsev[38,w], G. Manca[22,f], G. Mancinelli[6], D. Marangotto[21,q], J. Maratas[5,v], J.F. Marchand[4], U. Marconi[15], C. Marin Benito[7], M. Marinangeli[43], P. Marino[43], J. Marks[12], P.J. Marshall[54], G. Martellotti[26], M. Martin[6], M. Martinelli[42], D. Martinez Santos[41], F. Martinez Vidal[75], A. Massafferri[1], M. Materok[9], R. Matev[42], A. Mathad[50], Z. Mathe[42], C. Matteuzzi[20], A. Mauri[44], E. Maurice[7,b], B. Maurin[43], A. Mazurov[47], M. McCann[55,42], A. McNab[56], R. McNulty[13], J.V. Mead[54], B. Meadows[59], C. Meaux[6], N. Meinert[69], D. Melnychuk[31], M. Merk[27], A. Merli[21,q], E. Michielin[23], D.A. Milanes[68], E. Millard[50], M.-N. Minard[4], L. Minzoni[16,g], D.S. Mitzel[12], A. Mogini[8], R.D. Moise[55], J. Molina Rodriguez[1,y], T. Mombächer[10], I.A. Monroy[68], S. Monteil[5], M. Morandin[23], G. Morello[18], M.J. Morello[24,t], O. Morgunova[71], J. Moron[30], A.B. Morris[6], R. Mountain[61], F. Muheim[52], M. Mulder[27], C.H. Murphy[57], D. Murray[56], A. Mödden [10], D. Müller[42], J. Müller[10], K. Müller[44], V. Müller[10], P. Naik[48], T. Nakada[43], R. Nandakumar[51], A. Nandi[57], T. Nanut[43], I. Nasteva[2], M. Needham[52], N. Neri[21], S. Neubert[12], N. Neufeld[42], M. Neuner[12], R. Newcombe[55], T.D. Nguyen[43], C. Nguyen-Mau[43,n], S. Nieswand[9], R. Niet[10], N. Nikitin[35], A. Nogay[71], N.S. Nolte[42], D.P. O'Hanlon[15], A. Oblakowska-Mucha[30], V. Obraztsov[39], S. Ogilvy[18], R. Oldeman[22,f], C.J.G. Onderwater[70], A. Ossowska[29], J.M. Otalora Goicochea[2], P. Owen[44], A. Oyanguren[75], P.R. Pais[43], T. Pajero[24,t], A. Palano[14], M. Palutan[18], G. Panshin[74], A. Papanestis[51], M. Pappagallo[52], L.L. Pappalardo[16,g], W. Parker[60], C. Parkes[56], G. Passaleva[17,42], A. Pastore[14], M. Patel[55], C. Patrignani[15,e], A. Pearce[42], A. Pellegrino[27], G. Penso[26], M. Pepe Altarelli[42], S. Perazzini[42], D. Pereima[34], P. Perret[5], L. Pescatore[43], K. Petridis[48], A. Petrolini[19,h], A. Petrov[71], S. Petrucci[52], M. Petruzzo[21,q], B. Pietrzyk[4], G. Pietrzyk[43], M. Pikies[29], M. Pili[57], D. Pinci[26], J. Pinzino[42], F. Pisani[42],

JHEP03(2019)176

A. Piucci[12], V. Placinta[32], S. Playfer[52], J. Plews[47], M. Plo Casasus[41], F. Polci[8], M. Poli Lener[18], A. Poluektov[50], N. Polukhina[72,c], I. Polyakov[61], E. Polycarpo[2], G.J. Pomery[48], S. Ponce[42], A. Popov[39], D. Popov[47,11], S. Poslavskii[39], C. Potterat[2], E. Price[48], J. Prisciandaro[41], C. Prouve[48], V. Pugatch[46], A. Puig Navarro[44], H. Pullen[57], G. Punzi[24,p], W. Qian[64], J. Qin[64], R. Quagliani[8], B. Quintana[5], B. Rachwal[30], J.H. Rademacker[48], M. Rama[24], M. Ramos Pernas[41], M.S. Rangel[2], F. Ratnikov[37,ab], G. Raven[28], M. Ravonel Salzgeber[42], M. Reboud[4], F. Redi[43], S. Reichert[10], A.C. dos Reis[1], F. Reiss[8], C. Remon Alepuz[75], Z. Ren[3], V. Renaudin[7], S. Ricciardi[51], S. Richards[48], K. Rinnert[54], P. Robbe[7], A. Robert[8], A.B. Rodrigues[43], E. Rodrigues[59], J.A. Rodriguez Lopez[68], M. Roehrken[42], S. Roiser[42], A. Rollings[57], V. Romanovskiy[39], A. Romero Vidal[41], M. Rotondo[18], M.S. Rudolph[61], T. Ruf[42], J. Ruiz Vidal[75], J.J. Saborido Silva[41], N. Sagidova[33], B. Saitta[22,f], V. Salustino Guimaraes[63], C. Sanchez Gras[27], C. Sanchez Mayordomo[75], B. Sanmartin Sedes[41], R. Santacesaria[26], C. Santamarina Rios[41], M. Santimaria[18,42], E. Santovetti[25,j], G. Sarpis[56], A. Sarti[18,k], C. Satriano[26,s], A. Satta[25], M. Saur[64], D. Savrina[34,35], S. Schael[9], M. Schellenberg[10], M. Schiller[53], H. Schindler[42], M. Schmelling[11], T. Schmelzer[10], B. Schmidt[42], O. Schneider[43], A. Schopper[42], H.F. Schreiner[59], M. Schubiger[43], M.H. Schune[7], R. Schwemmer[42], B. Sciascia[18], A. Sciubba[26,k], A. Semennikov[34], E.S. Sepulveda[8], A. Sergi[47,42], N. Serra[44], J. Serrano[6], L. Sestini[23], A. Seuthe[10], P. Seyfert[42], M. Shapkin[39], Y. Shcheglov[33,†], T. Shears[54], L. Shekhtman[38,w], V. Shevchenko[71], E. Shmanin[72], B.G. Siddi[16], R. Silva Coutinho[44], L. Silva de Oliveira[2], G. Simi[23,o], S. Simone[14,d], I. Skiba[16], N. Skidmore[12], T. Skwarnicki[61], M.W. Slater[47], J.G. Smeaton[49], E. Smith[9], I.T. Smith[52], M. Smith[55], M. Soares[15], l. Soares Lavra[1], M.D. Sokoloff[59], F.J.P. Soler[53], F.L. Souza De Almeida[2], B. Souza De Paula[2], B. Spaan[10], E. Spadaro Norella[21,q], P. Spradlin[53], F. Stagni[42], M. Stahl[12], S. Stahl[42], P. Stefko[43], S. Stefkova[55], O. Steinkamp[44], S. Stemmle[12], O. Stenyakin[39], M. Stepanova[33], H. Stevens[10], A. Stocchi[7], S. Stone[61], B. Storaci[44], S. Stracka[24], M.E. Stramaglia[43], M. Straticiuc[32], U. Straumann[44], S. Strokov[74], J. Sun[3], L. Sun[66], K. Swientek[30], A. Szabelski[31], T. Szumlak[30], M. Szymanski[64], S. T'Jampens[4], Z. Tang[3], A. Tayduganov[6], T. Tekampe[10], G. Tellarini[16], F. Teubert[42], E. Thomas[42], J. van Tilburg[27], M.J. Tilley[55], V. Tisserand[5], M. Tobin[30], S. Tolk[42], L. Tomassetti[16,g], D. Tonelli[24], D.Y. Tou[8], R. Tourinho Jadallah Aoude[1], E. Tournefier[4], M. Traill[53], M.T. Tran[43], A. Trisovic[49], A. Tsaregorodtsev[6], G. Tuci[24,p], A. Tully[49], N. Tuning[27,42], A. Ukleja[31], A. Usachov[7], A. Ustyuzhanin[37], U. Uwer[12], A. Vagner[74], V. Vagnoni[15], A. Valassi[42], S. Valat[42], G. Valenti[15], R. Vazquez Gomez[42], P. Vazquez Regueiro[41], S. Vecchi[16], M. van Veghel[27], J.J. Velthuis[48], M. Veltri[17,r], G. Veneziano[57], A. Venkateswaran[61], M. Vernet[5], M. Veronesi[27], N.V. Veronika[13], M. Vesterinen[57], J.V. Viana Barbosa[42], D. Vieira[64], M. Vieites Diaz[41], H. Viemann[69], X. Vilasis-Cardona[40,m], A. Vitkovskiy[27], M. Vitti[49], V. Volkov[35], A. Vollhardt[44], D. Vom Bruch[8], B. Voneki[42], A. Vorobyev[33], V. Vorobyev[38,w], J.A. de Vries[27], C. Vázquez Sierra[27], R. Waldi[69], J. Walsh[24], J. Wang[61], M. Wang[3], Y. Wang[67], Z. Wang[44], D.R. Ward[49], H.M. Wark[54], N.K. Watson[47], D. Websdale[55], A. Weiden[44], C. Weisser[58], M. Whitehead[9], J. Wicht[50], G. Wilkinson[57], M. Wilkinson[61], I. Williams[49], M.R.J. Williams[56], M. Williams[58], T. Williams[47], F.F. Wilson[51], M. Winn[7], J. Wishahi[10], W. Wislicki[31], M. Witek[29], G. Wormser[7], S.A. Wotton[49], K. Wyllie[42], D. Xiao[67], Y. Xie[67], A. Xu[3], M. Xu[67], Q. Xu[64], Z. Xu[3], Z. Xu[4], Z. Yang[3], Z. Yang[60], Y. Yao[61], L.E. Yeomans[54], H. Yin[67], J. Yu[67,aa], X. Yuan[61], O. Yushchenko[39], K.A. Zarebski[47], M. Zavertyaev[11,c], D. Zhang[67], L. Zhang[3], W.C. Zhang[3,z], Y. Zhang[7], A. Zhelezov[12], Y. Zheng[64], X. Zhu[3], V. Zhukov[9,35], J.B. Zonneveld[52], S. Zucchelli[15]

[1] *Centro Brasileiro de Pesquisas Físicas (CBPF), Rio de Janeiro, Brazil*
[2] *Universidade Federal do Rio de Janeiro (UFRJ), Rio de Janeiro, Brazil*
[3] *Center for High Energy Physics, Tsinghua University, Beijing, China*

JHEP03(2019)176

[4] Univ. Grenoble Alpes, Univ. Savoie Mont Blanc, CNRS, IN2P3-LAPP, Annecy, France
[5] Clermont Université, Université Blaise Pascal, CNRS/IN2P3, LPC, Clermont-Ferrand, France
[6] Aix Marseille Univ, CNRS/IN2P3, CPPM, Marseille, France
[7] LAL, Univ. Paris-Sud, CNRS/IN2P3, Université Paris-Saclay, Orsay, France
[8] LPNHE, Sorbonne Université, Paris Diderot Sorbonne Paris Cité, CNRS/IN2P3, Paris, France
[9] I. Physikalisches Institut, RWTH Aachen University, Aachen, Germany
[10] Fakultät Physik, Technische Universität Dortmund, Dortmund, Germany
[11] Max-Planck-Institut für Kernphysik (MPIK), Heidelberg, Germany
[12] Physikalisches Institut, Ruprecht-Karls-Universität Heidelberg, Heidelberg, Germany
[13] School of Physics, University College Dublin, Dublin, Ireland
[14] INFN Sezione di Bari, Bari, Italy
[15] INFN Sezione di Bologna, Bologna, Italy
[16] INFN Sezione di Ferrara, Ferrara, Italy
[17] INFN Sezione di Firenze, Firenze, Italy
[18] INFN Laboratori Nazionali di Frascati, Frascati, Italy
[19] INFN Sezione di Genova, Genova, Italy
[20] INFN Sezione di Milano-Bicocca, Milano, Italy
[21] INFN Sezione di Milano, Milano, Italy
[22] INFN Sezione di Cagliari, Monserrato, Italy
[23] INFN Sezione di Padova, Padova, Italy
[24] INFN Sezione di Pisa, Pisa, Italy
[25] INFN Sezione di Roma Tor Vergata, Roma, Italy
[26] INFN Sezione di Roma La Sapienza, Roma, Italy
[27] Nikhef National Institute for Subatomic Physics, Amsterdam, Netherlands
[28] Nikhef National Institute for Subatomic Physics and VU University Amsterdam, Amsterdam, Netherlands
[29] Henryk Niewodniczanski Institute of Nuclear Physics Polish Academy of Sciences, Kraków, Poland
[30] AGH — University of Science and Technology, Faculty of Physics and Applied Computer Science, Kraków, Poland
[31] National Center for Nuclear Research (NCBJ), Warsaw, Poland
[32] Horia Hulubei National Institute of Physics and Nuclear Engineering, Bucharest-Magurele, Romania
[33] Petersburg Nuclear Physics Institute (PNPI), Gatchina, Russia
[34] Institute of Theoretical and Experimental Physics (ITEP), Moscow, Russia
[35] Institute of Nuclear Physics, Moscow State University (SINP MSU), Moscow, Russia
[36] Institute for Nuclear Research of the Russian Academy of Sciences (INR RAS), Moscow, Russia
[37] Yandex School of Data Analysis, Moscow, Russia
[38] Budker Institute of Nuclear Physics (SB RAS), Novosibirsk, Russia
[39] Institute for High Energy Physics (IHEP), Protvino, Russia
[40] ICCUB, Universitat de Barcelona, Barcelona, Spain
[41] Instituto Galego de Física de Altas Enerxías (IGFAE), Universidade de Santiago de Compostela, Santiago de Compostela, Spain
[42] European Organization for Nuclear Research (CERN), Geneva, Switzerland
[43] Institute of Physics, Ecole Polytechnique Fédérale de Lausanne (EPFL), Lausanne, Switzerland
[44] Physik-Institut, Universität Zürich, Zürich, Switzerland
[45] NSC Kharkiv Institute of Physics and Technology (NSC KIPT), Kharkiv, Ukraine
[46] Institute for Nuclear Research of the National Academy of Sciences (KINR), Kyiv, Ukraine
[47] University of Birmingham, Birmingham, United Kingdom
[48] H.H. Wills Physics Laboratory, University of Bristol, Bristol, United Kingdom
[49] Cavendish Laboratory, University of Cambridge, Cambridge, United Kingdom
[50] Department of Physics, University of Warwick, Coventry, United Kingdom
[51] STFC Rutherford Appleton Laboratory, Didcot, United Kingdom

JHEP03(2019)176

[52] School of Physics and Astronomy, University of Edinburgh, Edinburgh, United Kingdom
[53] School of Physics and Astronomy, University of Glasgow, Glasgow, United Kingdom
[54] Oliver Lodge Laboratory, University of Liverpool, Liverpool, United Kingdom
[55] Imperial College London, London, United Kingdom
[56] School of Physics and Astronomy, University of Manchester, Manchester, United Kingdom
[57] Department of Physics, University of Oxford, Oxford, United Kingdom
[58] Massachusetts Institute of Technology, Cambridge, MA, United States
[59] University of Cincinnati, Cincinnati, OH, United States
[60] University of Maryland, College Park, MD, United States
[61] Syracuse University, Syracuse, NY, United States
[62] Laboratory of Mathematical and Subatomic Physics, Constantine, Algeria, associated to [2]
[63] Pontifícia Universidade Católica do Rio de Janeiro (PUC-Rio), Rio de Janeiro, Brazil, associated to [2]
[64] University of Chinese Academy of Sciences, Beijing, China, associated to [3]
[65] South China Normal University, Guangzhou, China, associated to [3]
[66] School of Physics and Technology, Wuhan University, Wuhan, China, associated to [3]
[67] Institute of Particle Physics, Central China Normal University, Wuhan, Hubei, China, associated to [3]
[68] Departamento de Fisica, Universidad Nacional de Colombia, Bogota, Colombia, associated to [8]
[69] Institut für Physik, Universität Rostock, Rostock, Germany, associated to [12]
[70] Van Swinderen Institute, University of Groningen, Groningen, Netherlands, associated to [27]
[71] National Research Centre Kurchatov Institute, Moscow, Russia, associated to [34]
[72] National University of Science and Technology "MISIS", Moscow, Russia, associated to [34]
[73] National Research University Higher School of Economics, Moscow, Russia, Moscow, Russia
[74] National Research Tomsk Polytechnic University, Tomsk, Russia, associated to [34]
[75] Instituto de Fisica Corpuscular, Centro Mixto Universidad de Valencia — CSIC, Valencia, Spain, associated to [40]
[76] University of Michigan, Ann Arbor, United States, associated to [61]
[77] Los Alamos National Laboratory (LANL), Los Alamos, United States, associated to [61]

[a] Universidade Federal do Triângulo Mineiro (UFTM), Uberaba-MG, Brazil
[b] Laboratoire Leprince-Ringuet, Palaiseau, France
[c] P.N. Lebedev Physical Institute, Russian Academy of Science (LPI RAS), Moscow, Russia
[d] Università di Bari, Bari, Italy
[e] Università di Bologna, Bologna, Italy
[f] Università di Cagliari, Cagliari, Italy
[g] Università di Ferrara, Ferrara, Italy
[h] Università di Genova, Genova, Italy
[i] Università di Milano Bicocca, Milano, Italy
[j] Università di Roma Tor Vergata, Roma, Italy
[k] Università di Roma La Sapienza, Roma, Italy
[l] AGH — University of Science and Technology, Faculty of Computer Science, Electronics and Telecommunications, Kraków, Poland
[m] LIFAELS, La Salle, Universitat Ramon Llull, Barcelona, Spain
[n] Hanoi University of Science, Hanoi, Vietnam
[o] Università di Padova, Padova, Italy
[p] Università di Pisa, Pisa, Italy
[q] Università degli Studi di Milano, Milano, Italy
[r] Università di Urbino, Urbino, Italy
[s] Università della Basilicata, Potenza, Italy
[t] Scuola Normale Superiore, Pisa, Italy
[u] Università di Modena e Reggio Emilia, Modena, Italy

JHEP03(2019)176

[v] MSU — Iligan Institute of Technology (MSU-IIT), Iligan, Philippines
[w] Novosibirsk State University, Novosibirsk, Russia
[x] Sezione INFN di Trieste, Trieste, Italy
[y] Escuela Agrícola Panamericana, San Antonio de Oriente, Honduras
[z] School of Physics and Information Technology, Shaanxi Normal University (SNNU), Xi'an, China
[aa] Physics and Micro Electronic College, Hunan University, Changsha City, China
[ab] National Research University Higher School of Economics, Moscow, Russia

[†] Deceased

JHEP03(2019)176